Available online at www.sciencedirect.com
SCIENCE DIRECT®
Journal of Molecular Catalysis A: Chemical 225 (2005) 203–212
JOURNAL OF MOLECULAR CATALYSIS A: CHEMICAL
www.elsevier.com/locate/molcata

Efficient degradation of dye pollutants on nanoporous polyoxotungstate–anatase composite under visible-light irradiation

Yu Yang[a,1], Qingyin Wu[c], Yihang Guo[a], Changwen Hu[a,b,*], Enbo Wang[a]

[a] *Faculty of Chemistry, Northeast Normal University, Changchun 130024, PR China*
[b] *Department of Chemistry, Beijing Institute of Technology, Beijing 100081, PR China*
[c] *Department of Chemistry, Zhejiang University, Hangzhou 310027, PR China*

Received 8 July 2004; received in revised form 31 August 2004; accepted 31 August 2004
Available online 12 October 2004

Abstract

A novel photocatalyst, nanoporous anatase TiO_2 crystalline particles coupled by homogeneously dispersed Keggin unit, $H_3PW_{12}O_{40}/TiO_2$, was prepared by a simple and rapid process, i.e., at a lower temperature (200 °C) by combined sol–gel and programmed temperature hydrothermal methods. The resulting material was characterized by UV diffuse reflectant spectroscopy, XRD, ^{31}P MAS NMR, TEM, and nitrogen adsorption. This new photocatalyst exhibited visible-light photocatalytic activity to decompose 10 various organic dyes in aqueous systems. It was attempted to determine the feasibility of such a degradation by varying the chemical structures, either azoic (Congo Red (CR), Methyl Orange (MO), Ponceau G (PG), Orange II (OII), and Eriochrome Blue Black B (EB)), or anthraquinonic (Alizarin S (AS)), or heteropolyaromatic (Methylene Blue (MB)), or fluorescent (Neutral Red (NR), Rhodamine B (RB)), or sulfonic (Fuchsin Acid (FA)). The intermediates and the final products of degradation were detected by electrospray mass spectrometer (ES-MS) and ion chromatography (IC). According to the experimental results, we proposed a possible mechanism of the photodegradation of dyes under visible-light irradiation in the aqueous system.

Keywords: Photocatalysis; Anatase; Polyoxometalate; Nanoporous; Visible-light irradiation; Dye; Degradation

1. Introduction

Since the discovery of photoelectrochemical splitting of water on n-type TiO_2 electrodes [1], photochemistry has possessed many practical applications, such as in optoelectronic devices or in the field of industrial and environmental catalysis [2–7]. In recent years, two green photocatalysts now widely used are semiconductor metal oxides (mainly TiO_2 in the anatase phase) and polyoxometalates (POMs) [8–17]. Anatase TiO_2 has attracted much attention due to their efficient decomposition ability for organic pollutants under irradiation with UV light with wavelength shorter than 387 nm [18,19]. In the same way, many POM systems share the same general photochemical characteristics as the semiconductor photocatalysts due to their combination of physical and chemical properties, in terms of molecular and electronic versatility, reactivity, and stability [20,21]. But the problem is that only about 3% of solar spectrum falls in this UV range, whose energy exceeds the bandgap of the anatase crystalline phase or POMs (3.2 eV for anatase, and 4.6 eV for $[PW_{12}O_{40}]^{3-}$). In addition, both the ultrafine TiO_2 particles and soluble POM catalysts suffer from their inability to be recycled due to the milky dispersion with the aqueous reactants or high solubility in polar solvent [22]. All these restrict their technological applications on a large scale. The efficient use of the visible-light of the solar spectrum may then appear to be an appealing challenge for developing the future generation of photocatalytic materials. Attempts to increase the photocatalytic efficiency of titanium dioxide in visible region

* Corresponding author. Tel.: +86 10 82571381; fax: +86 10 82571381.
E-mail addresses: yangy364@nenu.edu.cn (Y. Yang), cwhu@bit.edu.cn (C. Hu).
[1] Tel.: +86 431 5269765; fax: +86 108 2571381.

1381-1169/$ – see front matter © 2004 Elsevier B.V. All rights reserved.
doi:10.1016/j.molcata.2004.08.031

have been made by doping other coupled semiconductor photocatalysts [23,24], coating and doping with transition metal and noble metal [25], and chemically modified TiO_2 by C or N to its reduced forms such as n-$TiO_{2-x}C_x$ or n-$TiO_{2-x}N_x$ [2,3,26]. Therefore, the charge separation in the photocarriers generation was enhanced, and the energy needed for photoexcitation was reduced, both of which make modified titanium dioxide possible to absorb light in the visible region.

In our previous work, a series of porous silica or titania (in the amorphous phase) materials impregnated with POMs have been prepared, and these hybrid catalysts present much higher photocatalytic activity than that of the starting POM, and being more easily handled for recycling use [20,21,27–29]. Considering the properties of titanium dioxide and POMs, in this paper, we first design and prepare nanoporous anatase TiO_2 crystalline particles coupled by homogeneously dispersed polyoxotungstate ($H_3PW_{12}O_{40}$) at a lower temperature (200 °C) via combination of the sol–gel technique with the programmed temperature hydrothermal method. The photocatalytic activity of $H_3PW_{12}O_{40}/TiO_2$ can be enhanced by: (a) the synergistic effect resulting from the combination of the starting polyoxotungstate and the anatase TiO_2 support [29]; (b) the bimodal porous structure (micro/mesoporosities); it can initiate the photochemical reactions under visible-light irradiation. Visible-light photocatalytic activity of the nanoporous polyoxotungstate–anatase composite was measured by the decomposition of various dyes (azoic, anthraquinonic, heteropolyaromatic, fluorescent, and sulfonic). The as-prepared material exhibited high photocatalytic activity for decomposition of dyes under visible-light irradiation. Meanwhile, it is easy to separate the catalyst for recycling uses after the reaction is finished, and almost identical dye conversions are achieved in the third runs, suggesting that the photocatalytic activity of the composite is stable under visible-light irradiation.

2. Experimental

2.1. Preparation and characterization of photocatalyst

A typical method of preparation of nanoporous $H_3PW_{12}O_{40}/TiO_2$ (PW_{12}/TiO_2) crystalline particles is described below. Titanium tetraisopropoxide (TTIP, 98%, 6 ml) was dissolved with 30 ml of iso-propyl alcohol while stirring was used. In another container, $H_3PW_{12}O_{40}$ (0.4 g) was dissolved with water (0.8 ml), and then added into the TTIP solution drop by drop. The resulting mixture was adjusted to pH 1–2 by addition of 8 mol/l HCl, and then stirred at room temperature for 1 h. Then, the mixture was heated to 45 °C until homogeneous $H_3PW_{12}O_{40}/TiO_2$ hydrogel formed. This hydrogel was transferred into an autoclave, and then heated to 200 °C at a heating rate of about 2 °C/min. Finally, the temperature was kept at 200 °C for 1 h. After cooling the hydrogel to room temperature, the hydrogel was dehydrated slowly at 50 °C in a vacuum for 24 h. The dried gel was washed with hot water three times, and then dried at room temperature. The product is white powder.

Elemental analysis was performed on a Leeman Plasma Spec (I) ICP-AES. DR UV–vis spectra were recorded on a Cary 500 UV–vis–NIR spectrometer. The XRD patterns were obtained with a Japan Rigaku D/max 2000 X-ray diffractometer with Cu Kα radiation (λ = 0.154178 nm). ^{31}P MAS NMR spectrum was obtained on a Varian Unity-400 NMR spectrometer. TEM and SAED measurements were carried out using a JEM-2010 microscope. BET specific surface area, pore size, and pore volume were calculated from nitrogen adsorption–desorption isotherms determined at 77 K using an ASAP 2010 surface analyzer (the sample was outgassed under vacuum at 200 °C).

2.2. Measurement of photocatalytic activity

The photoreactor was designed with cylindrical cell Pyrex glass configuration and an internal light source surrounded by a glass jacket, where the suspension of catalyst and aqueous dyes completely surrounded the light source. The temperature of suspension was maintained at 30 ± 2 °C by circulation of water through an external cooling coil. The light source was 400 W Xe lamp (λ > 420 nm).

The visible-light catalytic activity of the nanocomposite was tested using CR, MO, PG, OII, EB, AS, MB, NR, RB, and FA as the targets. A general photocatalytic procedure was carried out as follows: 0.25 g of catalyst $H_3PW_{12}O_{40}/TiO_2$ was suspended in a fresh aqueous dye solution (C_0 = 0.05 g/l, 200 ml). The suspension was ultrasonicated for 10 min and stirred in the dark for 30 min, and then the Xe lamp was inserted into the suspension after its intensity became stable. The suspension was vigorously stirred with the photoreactor open to air during the process.

At given intervals of illumination, a sample of PW_{12}/TiO_2 suspension was taken out and centrifuged. The upper clear solution was analyzed by UV–vis spectroscopy using a 756CRT UV–vis spectrophotometer. In situ FT-IR experiment was carried out by an Impact 410 FT-IR spectrometer with 256 scans at 4 cm^{-1} resolutions. An IR cell can be kept below 10^{-4} Torr by an oil-diffusion pump and mechanical pump. Some intermediates were identified by LQC ES-MS spectrometer and some final products were detected by a DX-300 IC equipped with a COM-Π conductivity detector.

3. Results and discussion

3.1. Properties of photocatalyst

Diffuse reflectance (DR) UV–vis spectra showed that the $H_3PW_{12}O_{40}/TiO_2$ crystallites exhibited broad and strong absorption in the range from 200 to 400 nm, which was different from the original $H_3PW_{12}O_{40}$ and anatase TiO_2 (Fig. 1). The red-shift (ca. 15 nm) was observed compared with the anatase support. The red-shift and widening of this band have been at-

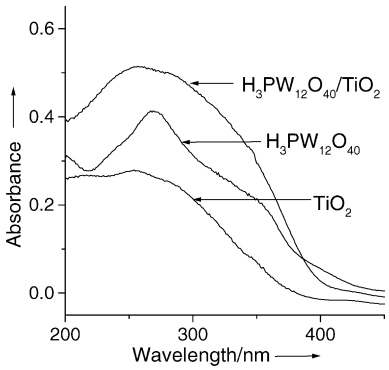

Fig. 1. DR–UV–vis spectra of $H_3PW_{12}O_{40}$, TiO_2 (anatase) support, and $H_3PW_{12}O_{40}/TiO_2$ (anatase) composite.

tributed to a distorted tetrahedral coordination environment or the existence of some titanium species in an octahedral coordination environment [30,31], i.e., the introduction of polyoxotungstate in TiO_2 framework results in the changes of coordination environment of TiO_2 crystalline.

Fig. 2A and B showed the X-ray diffraction (XRD) patterns of TiO_2 and $H_3PW_{12}O_{40}/TiO_2$ prepared via sol–gel following programmed temperature hydrothermal treatment have uniform anatase structure with its characteristic diffraction peaks of 2θ values at 25.3 (1 0 1), 37.8 (0 0 4), 48.0 (2 0 0), and 54.4 (1 0 5), 62.7° (2 1 1), respectively [32]. However, $H_3PW_{12}O_{40}/TiO_2$ particles prepared via only sol–gel method or sol–gel method following hydrothermal treatment without programmed temperature is amorphous (Fig. 2C). The precipitate derived by sol–gel method is amorphous in nature, requiring further heat treatment at a high temperature to induce crystallization. The thermal process results in particle agglomeration and grain growth, and hence may induce unexpected phase transformation [33–36]. At this considerably lower temperature (200 °C), the decomposition of the polyoxotungstate and the collapses of the pores can be avoided ($H_3PW_{12}O_{40}$ unit begins to decompose at ca. 350 °C [28], while the temperature for calcinations of amorphous TiO_2 to its anatase structure is at ca. 500 °C [37]). In Fig. 2B, only anatase phase was present in PW_{12}/TiO_2 nanoparticles and no separate polyoxotungstate-related phase was observed. This finding indicated that $H_3PW_{12}O_{40}$ was either in the octahedral interstitial sites or the substitutional positions of TiO_2 [38]. This XRD result is consistent with the conclusion obtained from the diffuse reflectance UV–vis spectra.

Elemental analysis for PW_{12}/TiO_2 (loading on the composition): P, 0.18%; W, 12.9%; PW_{12}, 19.6%, and the calculated P:W ratio from these data was ca. 1:12, suggesting the original Keggin unit existing in the PW_{12}/TiO_2 composite.

In order to further confirm the incorporation and connection of PW_{12} cluster with the titania framework, the PW_{12}/TiO_2 material was analyzed by solid-state ^{31}P magic-angle spinning (MAS) NMR. The PW_{12} cluster displayed a characteristic peak at δ −14.0 ppm (Fig. 3), which is different from the starting $H_3PW_{12}O_{40}$ (−15.0 ppm), suggesting that the acid–base interaction between $H_3PW_{12}O_{40}$ unit and the anatase matrix existing in the composite, resulting in ($\equiv TiOH_2^+$)($H_2PW_{12}O_{40}^-$) species [39]. The shift may be also due to the changes of the coordination environment of P atom in the composite.

Transmission electron microscopy (TEM) image showed the presence of uniform nanoparticles in the as-prepared composite (Fig. 4). The sizes of most particles in the product were found to be less than 10 nm. As we know, if the particle size becomes sufficiently small, quantum confinement of electron leads to a size-dependent separation between the valence and conduction bands, which are split into discrete exciton-like states [40]. The selected area electron diffraction (SAED) was perfect and showed that the composite has a uniform polycrystalline structure (inset in Fig. 4). The rings of the sample were indexed to diffraction from the (1 0 1), (0 0 4), (2 0 0), (1 0 5), (2 0 4), (1 1 6), and (2 1 5) planes of anatase, which were consistent with the XRD patterns depicted above.

Nitrogen adsorption–desorption analysis showed the composite was a novel bimodal pore system with micro/mesoporosities (Fig. 5). According to IUPAC definition, the isotherm of Fig. 5A belongs to type I, that is, a sharp increase in the adsorbed amount of N_2 at very low relative pressure (p/p_0 < 0.1) occurred. And the pore size was de-

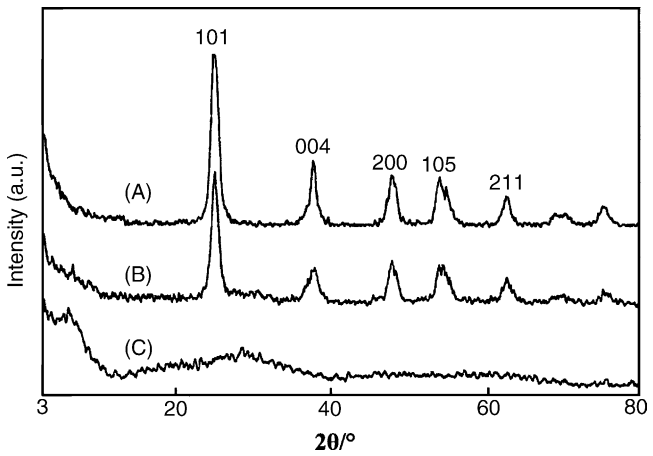

Fig. 2. XRD patterns for anatase TiO_2 (A), $H_3PW_{12}O_{40}/TiO_2$ (anatase) composite (B), amorphous $H_3PW_{12}O_{40}/TiO_2$ composite (C).

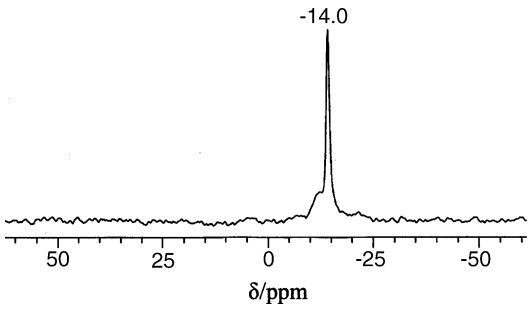

Fig. 3. ^{31}P MAS NMR spectrum of the $H_3PW_{12}O_{40}/TiO_2$ (anatase) composite.

Fig. 4. TEM image and SAED pattern (inset) of $H_3PW_{12}O_{40}/TiO_2$ (anatase) nanocomposite.

termined to be about 0.6 nm with narrow distribution using the BJH model (Fig. 5C). At the same time, we observed the isotherm of Fig. 5B is of type IV and shows steep hysteresis loop at high relative pressure, which is typical of mesoporous materials with pore size of about 4.0 nm (Fig. 5D). Formation of micropores in the product is directly related to the preparation method used here. That is, during the process of hydrolysis of titanium tetraisopropoxide (TTIP) in the presence of $H_3PW_{12}O_{40}$, the Keggin units were entrapped by the titania network and entered its pore to interact with its internal surface hydroxyl groups of Ti (≡Ti–OH), resulting in

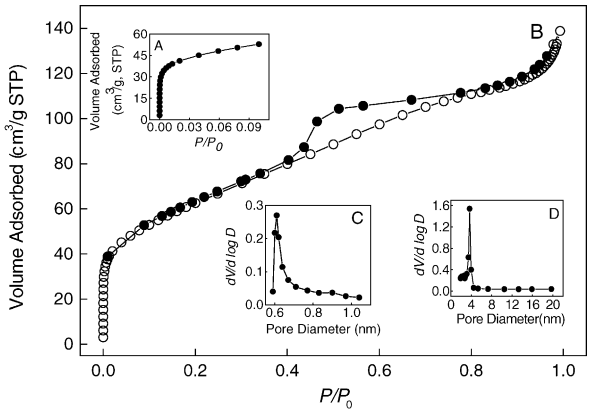

Fig. 5. Nitrogen adsorption–desorption isotherm and pore size distributions for $H_3PW_{12}O_{40}/TiO_2$ (anatase) hybrid. (A): Isotherm of type I; (B): isotherm of type IV; (C): micropore size distribution; (D): mesopore size distribution.

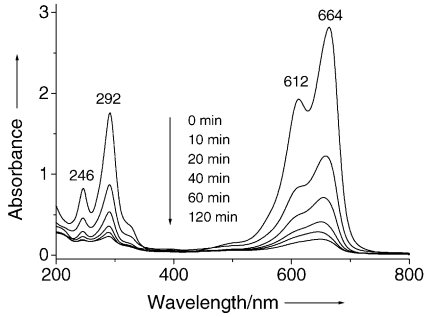

Fig. 6. UV–vis spectral changes of MB (0.05 g/l, 200 mL) on $H_3PW_{12}O_{40}/TiO_2$ (0.25 g, anatase phase) composite with visible-light irradiation time.

the ($\equiv TiOH_2^+$)($H_2PW_{12}O_{40}^-$) composite with the decrease of the pore size of the titania network. In this composite, hydrogen bonds such as W=O_t···HO–Ti, W–O_c···HO–Ti, and W–O_e···HO–Ti also formed between the oxygen atoms of Keggin ion and the ≡Ti–OH groups of titania network. Subsequent dehydration is also necessary to ensure Keggin units were entrapped into the pore of titania network. And some internal surface of titanium dioxide framework that did not entrap the Keggin ions would still retain the mesoporous structures. Moreover, the BET surface area of PW_{12}/TiO_2 was 201 $m^2\ g^{-1}$, which was improved greatly compared with both the starting polyoxotungstates (<10 $m^2\ g^{-1}$) and the Degussa P25 (50 $m^2\ g^{-1}$) [32].

3.2. Studies of visible-light catalytic degradation of dyes

3.2.1. Photocatalytic activity

We studied the degradation of methylene blue (MB) as a model reaction to investigate the photocatalytic activity of PW_{12}/TiO_2 and the degradation mechanism on this catalyst under visible-light irradiation. MB is a heteropolyaromatic dye, and the structure of MB is illustrated in Table 1. The present photocatalytic tests were run in aqueous solution containing molecule oxygen from air dissolved in solution. The changes in the concentration of MB recorded following UV–vis irradiation are shown in Figs. 6 and 7. The results

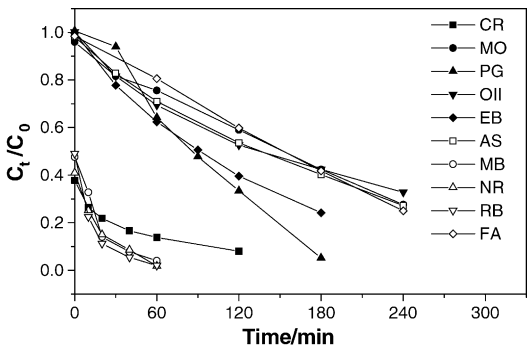

Fig. 7. Concentrations of different dyes changes as a function of visible-light irradiation time.

Table 1
Characteristics of 10 dyes photocatalytically degraded under visible-light irradiation

Dye	Chemical formula	MW (g/mol)	λ_{max} (nm)
Congo Red (CR)	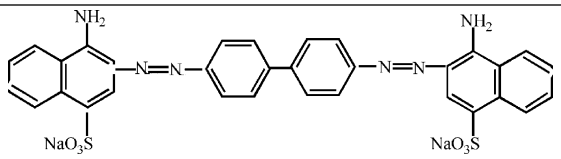	696.67	498
Methyl Orange (MO)	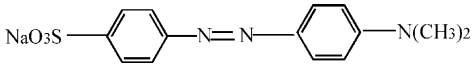	327.34	464
Ponceau G (PG)	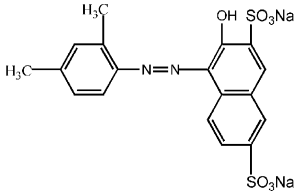	480.42	507
Orange II (OII)	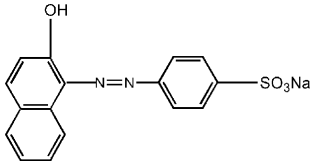	440.40	482
Eriochrome Blue Black B (EB)	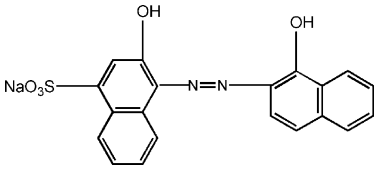	416.40	619
Alizarin S (AS)	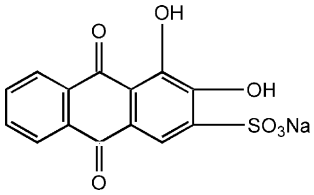	360.28	520
Methylene Blue (MB)	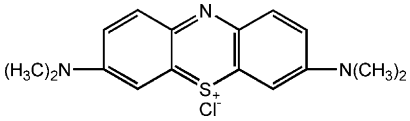	373.88	664
Neutral Red (NR)	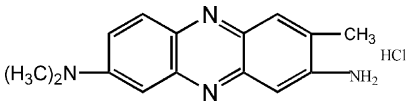	288.78	525
Rhodamine B (RB)	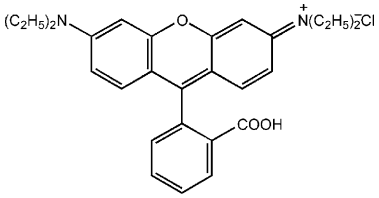	479.28	554
Fuchsin Acid (FA)	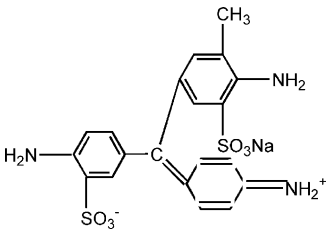	585.58	544

obtained in the process of photocatalytic degradation of MB are summarized as follows.

On stirring the suspension of aqueous MB solution (50 mg/l or 0.14 mmol/l, 200 ml) without catalyst in the dark for 5 h, the disappearance of MB was negligible. In addition, the MB solution without catalyst is directly photolyzed under visible-light irradiation for 5 h, and the conversion of MB was only 15%. However, the conversion of MB was much higher when visible-light irradiation was applied in the presence of PW_{12}/TiO_2 (0.25 g), namely, the conversion of MB reached 96% after 60 min visible-light irradiation (Fig. 6). When the as-prepared anatase TiO_2 (0.25 g) was used as catalyst, the MB conversion was less than 40% in the same time, and the milky dispersion with the aqueous reactant was unable to separate and recycle. These data illustrate that the visible-light photocatalytic activity of PW_{12}/TiO_2 is higher than that of the traditional anatase TiO_2 catalyst, and it suggests that the degradation of MB mainly originated from the synergistic effect yielded by the combination of PW_{12} and TiO_2. The synergistic effect is that in the system of anatase TiO_2 crystalline particles coupled by homogeneously dispersed Keggin units, the interfacial electron transfer takes place from the TiO_2 conduction to PW_{12} after visible-light irradiation. Such an effective electron transfer can inhibit the fast electron–hole recombination on TiO_2, and the trapped holes have sufficient time to react with H_2O to generate $OH^\bullet$ radicals. The $OH^\bullet$ radicals photo-oxidized MB, resulting in the decolorization of the solution [29]. Pure anatase TiO_2 has no the synergistic effect, therefore the interfacial electron transfer takes place in TiO_2 itself, resulting in the fast electron–hole recombination. Therefore, the photocatalytic efficiency of anatase TiO_2 under visible-light irradiation was lower.

This high photocatalytic activity is also attributed to the bimodal porous structure of the $H_3PW_{12}O_{40}/TiO_2$ nanocomposite. First, it provides enhanced mass transport for molecules into and out of the pore structure. Second, we noted that the concentration of MB decreased by ca. 55% before visible-light irradiation (Fig. 7), suggesting that strong adsorption of the reactants occurred (the adsorption reached equilibrium after stirring the suspension for 30 min). With large surface area, the composite exhibited a binary function for degradation of MB through both photocatalysis and adsorption, which played important roles to decompose the MB molecules.

After the reaction finished, the suspension was centrifuged, and the catalyst $H_3PW_{12}O_{40}/TiO_2$ was separated. The amount of W determined by ICP-AES in the resulting clear solution was 0.2%, which confirmed the less solubility of the catalyst during the reaction process. After treated, the catalyst was reused in the photocatalytic experiment. The catalytic activity of $H_3PW_{12}O_{40}/TiO_2$ in the degradation of MB was maintained efficiently after three repeated experiments (Fig. 8). In addition, the catalyst can be separated from the solution simply by settlement, which is better than the traditional TiO_2 system.

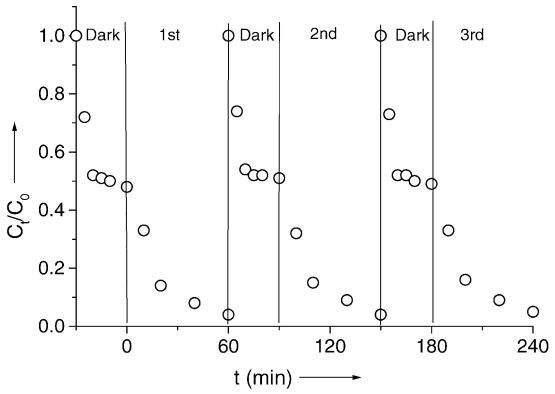

Fig. 8. Cycling runs in the photodegradation of MB in the presence of $H_3PW_{12}O_{40}/TiO_2$ (anatase) under visible-light irradiation.

In order to sufficiently test the efficiency of the degradation and decolorizaton of this new catalyst for organic dye pollutants, we chose other nine colorful dyes including azoic (CR, MO, PG, OII, and EB), anthraquinonic (AS), fluorescent (NR and RB), and sulfonic (FA). Their structures and other details are listed in Table 1. In particular, we selected 5 azo dyes as reactants. Azo dyes are abundant class of synthetic, colored, organic compounds, which are characterized by the presence of one or more azo bonds (–N=N–) [41]. Bio-treatment of azo dyes is, in general, ineffective, due to their resistance to aerobic degradation, which represent an increasing environmental danger. The other four dyes represent different types including anthraquinonic, heteropolyaromatic, fluorescent and sulfonic. The degradation processes were controlled by monitoring the absorbance characteristics of the targets at λ_{max}, and the results were shown in Fig. 7. From Fig. 7, we observed the concentrations decrease by ca. 50% before visible-light irradiation for CR, MB, NR, and RB, which suggested the strong adsorption of these reactants, occurred on the surface of the catalyst, and the dye molecules can easily react with the catalyst, resulting in the higher conversion in the shorter reaction time. The adsorptions of other six dyes (MO, PG, OII, EB, AS, and FA) were weaker, and the conversions were lower accordingly. The detailed reaction conditions, conversions and reaction rates were listed in Table 2. In the main, the higher the conversion, the faster the initial rate is. But the conversion of CR is high, and its initial rate is slow. It was possibly because the CR molecule with large and complicated structure was hardly degraded.

3.2.2. Photocatalytic kinetics

We selected MB as reference to investigate the kinetics of dye degradation in aqueous solution under visible-light irradiation, and the results were shown on Fig. 9. It follows an apparent first-order in agreement with a generally observed Langmuir–Hinshelwood kinetics model:

$$r = \frac{dC}{dt} = \frac{kKC}{1 + KC} \quad (1)$$

Table 2
Visible-light photocatalytic activity of the nanoporous polyoxotungstate–anatase composite for organic dyes degradation

Substrate[a]	Time (min)	Conversion (%)[b]	Initial rate ($mg\,l^{-1}\,min^{-1}$)[c]
CR	120	92	0.18
MO	240	72.4	0.17
PG	180	94.8	0.30
OII	240	67.2	0.26
EB	180	75.8	0.31
AS	240	72.8	0.23
MB	60	96	0.35
NR	60	98.2	0.30
RB	60	98	0.34
FA	240	75	0.15

[a] The concentration of substrate was 50 mg/l, the weight of catalyst PW_{12}/TiO_2 was 0.25 g, and the reaction occurred under visible-light irradiation ($\lambda > 420$ nm) at room temperature, and the system was open to air.

[b] Conversion (%) = $(1 - C_t/C_0) \times 100$; C_0 and C_t = concentration of the substrate at times 0 and t (C_0 = 50 mg/l).

[c] The initial rate is defined that the decrease of substrate concentration in the initial 60 min ($\gamma = -dc/dt$, $mg\,l^{-1}\,min^{-1}$, considering the adsorption of the substrate).

where r is the degradation rate of the reactant (mg/l min), C the concentration of the reactant (mg/l), t the illumination time, k the reaction rate constant (mg/l min), and K the adsorption coefficient of the reactant (l/mg).

When the initial concentration C_0 is micromolar solution (C_0 = 66.6 μmol/l in the present experiment), the Eq. (1) can be simplified to an apparent first-order equation:

$$\ln\left(\frac{C_0}{C}\right) = kKt = k_{app}t \quad (2)$$

A plot of $\ln C_0/C$ versus time represents a straight line, the slope of which upon linear regression equals the apparent first-order rate constant k_{app} (0.044 min^{-1}).

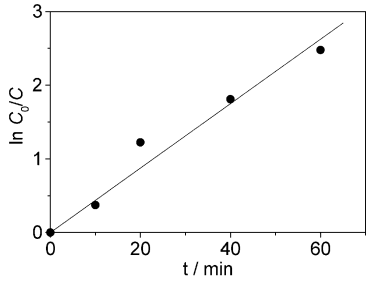

Fig. 9. First-order linear $\ln C_0/C = f(t)$. Conditions: C_0 = 66.6 μmol/l; $m(H_3PW_{12}O_{40}/TiO_2)$ = 0.25 g; V = 200 ml.

3.2.3. Photocatalytic mechanism

In the direct photocatalysis, both positive holes and hydroxyl radicals have been proposed as the oxidizing species responsible for initiating the degradation of the organic substrates [18,19,42,43]. Two possible mechanisms have been proposed. The first mechanism is that when photocatalytic oxidation is conducted in the presence of water, the holes were

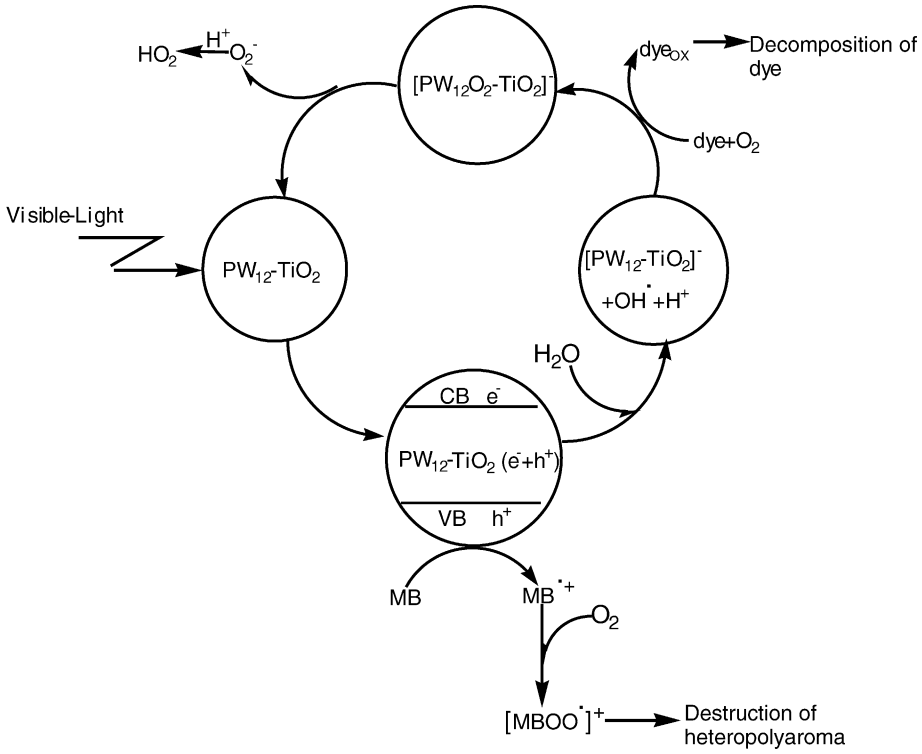

Scheme 1. Proposed photodegradation mechanism of dyes in the presence of $H_3PW_{12}O_{40}/TiO_2$.

efficiently scavenged by water and generated hydroxyl radicals $OH^{\bullet}$, which are strong and unselected oxidant species in favor of totally oxidative degradation and mineralization for organic substrates. The second one is that substrates (dyes) with the proper oxidation potential can undergo direct oxidation, and generate radical species. In our system, we proposed a possible dye photocatalytic degradation mechanism according to the above experimental results, which was confirmed by in situ FT-IR result (Scheme 1). In the photocatalysis, the $H_3PW_{12}O_{40}/TiO_2$ nanocomposite absorbed visible-light to produce electron/hole (e^-/h^+) pairs. Some organic dyes can be strongly absorbed on the $H_3PW_{12}O_{40}/TiO_2$ surface. For example, MB is mainly oxidized by photogenerated hole localized on the surface of the irradiated catalyst, generated an adsorbed MB cation radical ($MB^{\bullet+}$). The MB cation radical formed combines with molecular oxygen and results in the destruction of heteropolyaromatic. The active oxygen species produced during this photocatalysis process was superoxide species ($O_2^{\bullet-}$), which was confirmed by in situ FT-IR spectrum (Fig. 10). That is, IR spectrum of adsorbed O_2 at room temperature on the composite is shown in Fig. 10. The band at 837 cm^{-1} for $^{16}O_2$ adsorption was clearly observed after admission of $^{16}O_2$ to the system of PW_{12}/TiO_2 and aqueous MB (Fig. 10B). This band is originated from a peroxo-bond (O–O) stretching vibration [44]. For other dyes adsorbed less

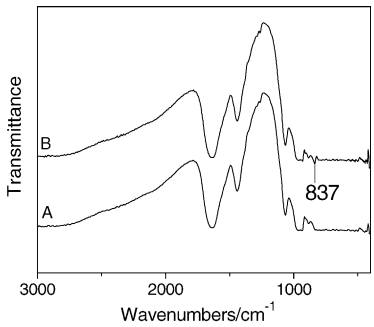

Fig. 10. In situ IR spectra of the $H_3PW_{12}O_{40}/TiO_2$ composite (A) and adsorbed dioxygen on the composite at 298 K after admission of O_2 (30 Torr) for 1 min (B).

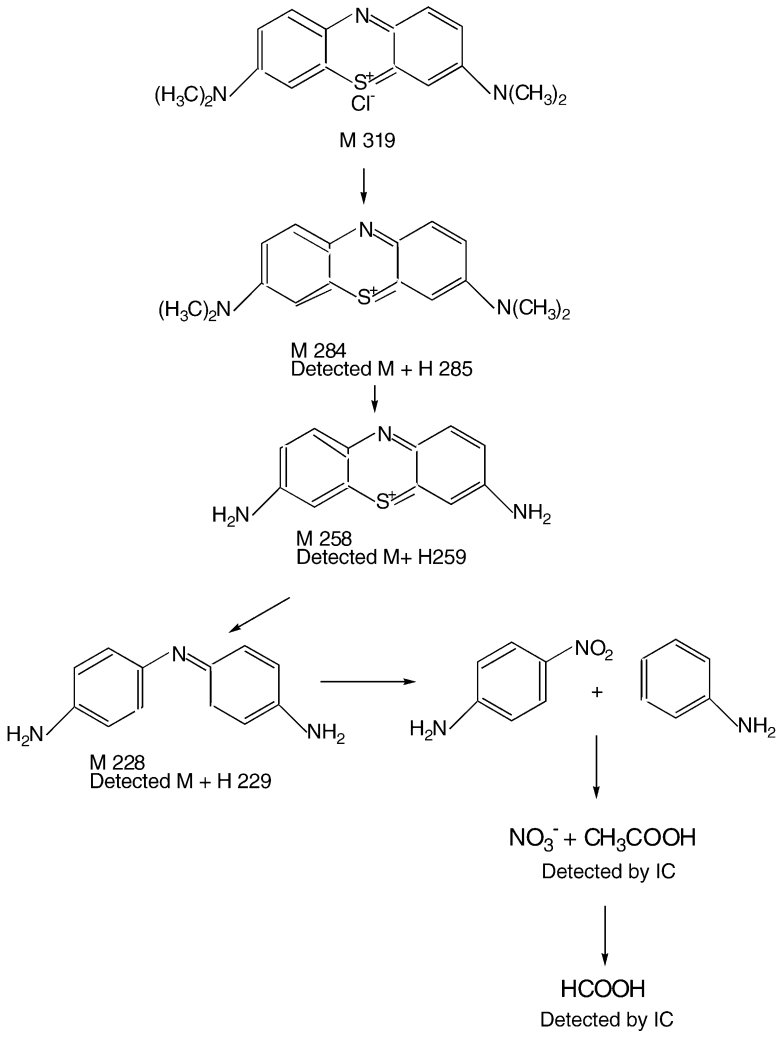

Scheme 2. Photocatalytic degradation pathway of MB in the presence of $H_3PW_{12}O_{40}/TiO_2$.

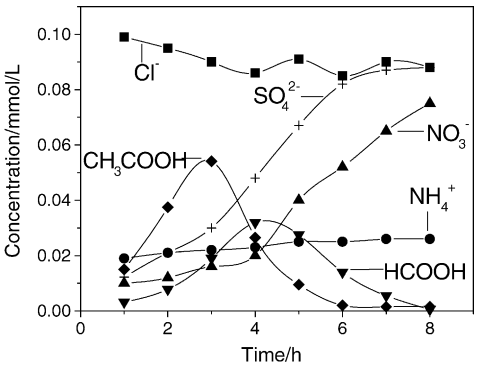

Fig. 11. Evolution of NH_4^+, SO_4^{2-}, NO_3^-, Cl^-, acetic acid and formic acid in solution during photocatalytic degradation of MB (C_0 = 0.14 mmol/L).

on the catalyst, the photogenerated holes reacted with water molecules to produce hydroxyl radicals, and the hydroxyl radicals attacked dye molecules. Finally, the dyes were oxidized and subsequently degraded to small species.

3.2.4. Photodegradation pathway

These degraded species of MB can be detected by ES-MS and IC. According to the intermediates and final products detected, we proposed a possible degradation pathway in Scheme 2. Successive degradation main steps of MB may occur as follows: (i) cleavage of C–N bond of the substituting group of the heteropolyaromatic; (ii) desulfurization; (iii) cleavage of C–N bond of heteropolyaromatic; (iv) cleavage of C–C bond of aromatic ring.

Evolutions of some intermediates such as formic acid and acetic acid, and inorganic ions such as NH_4^+, SO_4^{2-}, NO_3^-, Cl^- as a function of irradiation time are shown in Fig. 11. It can be seen that the amount of SO_4^{2-} and NO_3^- ions increased gradually as the irradiation time increasing, indicating that MB was mineralized. As for NH_4^+ ion, the amount was not too big and the change was neglectable. The result indicated that the transformation from NH_4^+ to NO_3^- occurred when NH_4^+ ion generated. After ca. 7 h irradiation, acetic acid disappeared, and then formic acid after another 1 h irradiation, indicating that mineralization of MB into CO_2 is completely after 8 h irradiation in the presence of PW_{12}/TiO_2.

4. Conclusion

This work introduces a simple and green heterogeneous photocatalytic approach for the degradation of organic pollutants. The preparation of highly crystalline polyoxotungstate–anatase nanoporous composite by combined sol–gel and programmed temperature hydrothermal methods can be controlled easily at lower temperature (200 °C). The obtained composite exhibited both nanoparticle and unique bimodal porous structure and showed visible-light photocatalytic activity for decomposition of several sorts of dyes; meanwhile, it is easy to separate the catalysts for recycling uses after the reaction is finished. The mechanism of photodegradation of organic pollutants on the as-prepared catalyst under visible-light irradiation was due to $O_2^{\bullet-}/OH^{\bullet}$. The application of as-prepared material exhibits a potential for the treatment of dye pollutants because it can fully utilize solar radiation. The present work also provides useful insight for the development of a new route in synthetic chemistry.

Acknowledgments

The Natural Science Foundation Council of China is acknowledged for financial support (20271007, 20331010 and 20271045). The present work is also supported by Specialized Research Fund for the Doctoral Program of Higher Education (20030007014). We thank Professor F. Xiao for helpful discussions.

References

[1] A. Fujishima, K. Honda, Nature 238 (1972) 37.
[2] R. Asahi, T. Morikawa, T. Ohwaki, K. Aoki, Y. Taga, Science 293 (2001) 269.
[3] S.U.M. Khan, M. Al-Shahry, W.B. Ingler Jr., Science 297 (2002) 2243.
[4] W. Ma, J. Li, X. Tao, J. He, Y. Xu, J.C. Yu, J. Zhao, Angew. Chem. Int. Ed. 42 (2003) 1029.
[5] Z. Zou, J. Ye, K. Sayama, H. Arakawa, Nature 414 (2001) 625.
[6] H. Murayama, K. Shimizu, N. Tsukada, A. Shimada, T. Kodama, Y. Kitayama, Chem. Commun. (2002) 2678.
[7] D. Sattari, C.L. Hill, J. Am. Chem. Soc. 115 (1993) 4649.
[8] C.L. Hill, D.A. Bouchard, M. Kadkhodayan, M.M. Williamson, J.A. Schmidt, E.F. Hilinski, J. Am. Chem. Soc. 110 (1988) 5471.
[9] B.S. Jaynes, C.L. Hill, J. Am. Chem. Soc. 117 (1995) 4704.
[10] E. Papaconstantinou, Chem. Soc. Rev. 18 (1989) 1.
[11] L. Ermolenko, C. Giannotti, J. Mol. Catal. A: Chem. 114 (1996) 87.
[12] C. Tanielian, R. Seghrouchni, C. Schweitzer, J. Phys. Chem. A 107 (8) (2003) 1102.
[13] T. Yamase, E. Ishikawa, Langmuir 16 (23) (2000) 9023.
[14] T. Yamase, Chem. Rev. 98 (1998) 307.
[15] A. Mills, S. Le Hunte, J. Photochem. Photobiol. A 108 (1997) 1.
[16] P.V. Kamat, Chem. Rev. 93 (1993) 267.
[17] H. Hidaka, S. Horikoshi, K. Ajiaka, J. Zhao, N. Serpone, J. Photochem. Photobiol. A 108 (1997) 197.
[18] M.A. Fox, M.T. Dulay, Chem. Rev. 93 (1993) 341.
[19] M.R. Hoffmann, S.T. Martin, W. Chio, D.W. Bahnemann, Chem. Rev. 95 (1995) 69.
[20] Y. Guo, C. Hu, S. Jiang, C. Guo, Y. Yang, E. Wang, Appl. Catal. B 36 (2002) 9.
[21] Y. Guo, C. Hu, X. Wang, E. Wang, Y. Zhou, S. Feng, Chem. Mater. 3 (2001) 4058.
[22] K.Y. Lee, T. Arai, S. Nakata, S. Asaoka, T. Okuhara, M. Misono, J. Am. Chem. Soc. 114 (1992) 2836.
[23] J. Engweiler, J. Harf, A. Baiker, J. Catal. 159 (1996) 259.
[24] S.K. Poznyak, D. Talapin, A. Kulak, J. Phys. Chem. B 105 (2001) 4816.
[25] W. Choi, A. Termin, M.R. Hoffmann, J. Phys. Chem. 98 (1994) 13669.
[26] I. Justicia, P. Ordejón, G. Canto, J.L. Mozos, J. Fraxedas, G.A. Battiston, R. Gerbasi, A. Figueras, Adv. Mater. 14 (2002) 1399.
[27] Y. Guo, C. Hu, C. Jiang, Y. Yang, S. Jiang, X. Li, E. Wang, J. Catal. 217 (2003) 141.

[28] Y. Guo, Y. Yang, C. Hu, C. Guo, E. Wang, Y. Zhou, S. Feng, J. Mater. Chem. 12 (2002) 3046.
[29] Y. Yang, Y. Guo, C. Hu, C. Jiang, E. Wang, J. Mater. Chem. 13 (2003) 1686.
[30] W. Zhang, J. Lu, B. Han, M. Li, J. Xiu, P. Ying, C. Li, Chem. Mater. 14 (2002) 3413.
[31] T. Blasco, A. Corma, M. Navarro, J. Pariente, J. Catal. 156 (1995) 65.
[32] H. Zhu, J.A. Orthman, J. Li, J. Zhao, G. Churchman, E. Vansant, Chem. Mater. 14 (2002) 5037.
[33] M. Kang, Appl. Catal. B 37 (2002) 187.
[34] L. Lei, H.P. Chu, X. Hu, P.L. Yue, Ind. Eng. Chem. Res. 38 (1999) 3381.
[35] T. Noguchi, A. Fujishma, Environ. Sci. Technol. 32 (1998) 3831.
[36] C.R. Peterson, E.B. Slamorich, J. Am. Ceram. Soc. 82 (1999) 241.
[37] X. Jiang, T. Herricks, Y. Xia, Adv. Mater. 15 (2003) 1205.
[38] S.I. Shah, W. Li, C.P. Huang, O. Jung, C. Ni, PNAS 99 (2002) 6482.
[39] I.V. Kozhevniikov, Chem. Rev. 98 (1998) 171.
[40] L.M. Peter, D.J. Riley, E.J. Tull, K.G.U. Wijayantha, Chem. Commun. (2002) 1030.
[41] M. Stylidi, D.I. Kondarides, X.E. Verykios, Appl. Catal. B 40 (2003) 271.
[42] G.M. Liu, J.C. Zhao, New J. Chem. 24 (2000) 411.
[43] M. Chio, M.R. Hoffmann, J. Phys. Chem. 100 (1996) 2161.
[44] Z.W. Xi, N. Zhou, Y. Sun, K.L. Li, Science 292 (2001) 1139.